STUDY ON EXTRACTION PARAMETERS OF FLUTTER DERIVATIVES FOR THE DEVELOPMENT OF A TIME-DOMAIN FORMULATION OF SELF-EXCITED FORCES

Sébastien MAHEUX[1], Sébastien LANGLOIS[1], Frédéric LÉGERON[2]
[1]Department of Civil Engineering, Université de Sherbrooke – Canada
sebastien.m.maheux@usherbrooke.ca
[2]Parsons – United Arab Emirates

Abstract

This paper addresses the evaluation of the dependence of bridge-deck flutter derivatives to the extraction parameters used in wind tunnel tests. The studied parameters are the model scale, model velocity and amplitude of motion. The measurements of flutter derivatives for the Great Belt Bridge were done through forced-vibration tests. This research shows that the flutter derivatives measured for different model scales have similar trends. Some derivatives show a dependence with respect to the amplitude. When studied in their dimensional form, the flutter derivatives H_5^*, A_5^*, H_2^* *and* A_2^* *exhibit nonlinearities for the velocity. Therefore, the study of a new nondimensionalization for the flutter derivatives based on the velocity would be interesting for the development of a new time-domain formulation of self-excited forces.*

INTRODUCTION

Slender bridges, such as suspension and cable-stayed bridges, are flexible structures that are effective to resist earthquakes, but their flexibility makes them vulnerable to wind actions, such as the flutter instability. Flutter is an aeroelastic instability caused by an interaction between wind and bridge-deck motions. This instability can cause major damages and even a total collapse. The assessment of flutter is done by the analysis of self-excited forces, i.e., forces resulting from deck motions. Scanlan's formulation of self-excited forces is widely used for this purpose [1]. This force model is based on the flutter derivatives, which are experimental coefficients obtained from wind tunnel tests. From the fact that the flutter derivatives are functions of the reduced frequency, the use of Scanlan's formulation is limited to linear analyses.

However, slender bridges are nonlinear structures because of the geometrical nonlinearities of the cables. Material nonlinearities of the bridge structure can also arise from the large displacements of the deck associated with wind loads. Additionally, the self-excited forces show aerodynamic nonlinearities. Some researchers demonstrate the dependence of flutter derivatives with respect to the amplitude of motion of the bridge deck [2-4]. The flutter derivatives also exhibit a nonlinear behavior for the frequency of oscillation [4]. Including these nonlinearities in flutter analysis would lead to more realistic flutter predictions for cable-supported bridges. To do so, the development of a new time-domain model of self-excited forces will be pertinent. Prior to the development of a new time-domain approach, it is relevant to have a better understanding of the dependence of flutter derivatives with respect to the extraction parameters.

For this reason, this paper addresses the evaluation of the model scale, model velocity, which is a time-domain parameter, and the amplitude of motion on the flutter derivatives of Scanlan's formulation. To achieve this objective, the flutter derivatives of the Great Belt Bridge were measured in the wind tunnel using the forced-vibration procedure. By extracting the derivatives for multiple values of the extraction parameters, the effect on the flutter derivatives of each parameter can be evaluated.

SCANLAN'S FORMULATION

The reference system used in this research for the self-excited forces is shown in Fig. 1. Eqs. 1-3 present Scanlan's form of self-excited forces employed in this investigation on the extraction parameters [5].

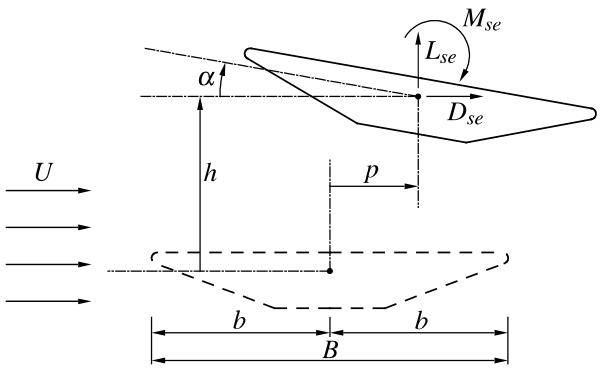

FIGURE 1 - Self-excited forces on a bridge deck

$$D_{se}(t)=\frac{1}{2}\rho U^2(2b)\left(kP_1^*\frac{\dot{p}}{U}+kP_2^*\frac{b\dot{\alpha}}{U}+k^2P_3^*\alpha+k^2P_4^*\frac{p}{b}+kP_5^*\frac{\dot{h}}{U}+k^2P_6^*\frac{h}{b}\right) \tag{1}$$

$$L_{se}(t)=\frac{1}{2}\rho U^2(2b)\left(kH_1^*\frac{\dot{h}}{U}+kH_2^*\frac{b\dot{\alpha}}{U}+k^2H_3^*\alpha+k^2H_4^*\frac{h}{b}+kH_5^*\frac{\dot{p}}{U}+k^2H_6^*\frac{p}{b}\right) \tag{2}$$

$$M_{se}(t)=\frac{1}{2}\rho U^2(2b^2)\left(kA_1^*\frac{\dot{h}}{U}+kA_2^*\frac{b\dot{\alpha}}{U}+k^2A_3^*\alpha+k^2A_4^*\frac{h}{b}+kA_5^*\frac{\dot{p}}{U}+k^2A_6^*\frac{p}{b}\right) \tag{3}$$

where $D_{se}(t)$, $L_{se}(t)$ and $M_{se}(t)$ are the self-excited forces; t is the time; ρ is the density of air; U is the mean wind speed; b is the half of the bridge-deck width B; $k=\omega b/U$ is the reduced frequency; ω is the angular frequency of oscillation; P_i^*, H_i^* and A_i^* ($i=1,\ldots,6$) are the flutter derivatives, which are functions of the reduced velocity $U_R=U/fB$; f is the frequency of oscillation; $p=p(t)$, $h=h(t)$ and $\alpha=\alpha(t)$ are the horizontal, vertical and rotational displacements; the overdot denotes the time derivative.

EXPERIMENTAL PROGRAM

Facilities

For the identification of flutter derivatives, section model tests were performed in the main wind tunnel of the *Université de Sherbrooke*, which is a closed return tunnel with a maximum wind speed of

31 m/s. The 10-m-long test section is 1.83 m by 1.83 m. Bridge models are positioned 7 m downwind of the outlet of the wind tunnel contraction. The velocity profile at this location is uniform within ±1.5 %, and a turbulence intensity of 1.2 % was measured. For the section model tests, the mean wind speed was measured with two Pitot tubes located above and below the model at its leading edge (Fig. 2a). A third Pitot tube positioned 4.6 m upwind the section model was also used as a reference only.

As shown in Fig. 2, the model was mounted on a three-degree-of-freedom (DOF) aerodynamic balance, which is described in [6]. In order to perform forced-vibration tests, six computer-controlled hydraulic actuators (MTS 242.01) were used to impose a motion to the model (Fig. 2b). The imposed displacements and the associated forces were measured using respectively six laser displacement sensors (Sunx LM10) and 24 load cells (FUTEK LCM300). A sampling rate of 200 Hz was employed for the measurements. More information can be found in [7-8] on the use of this experimental rig for the identification of flutter derivatives through forced-vibration tests.

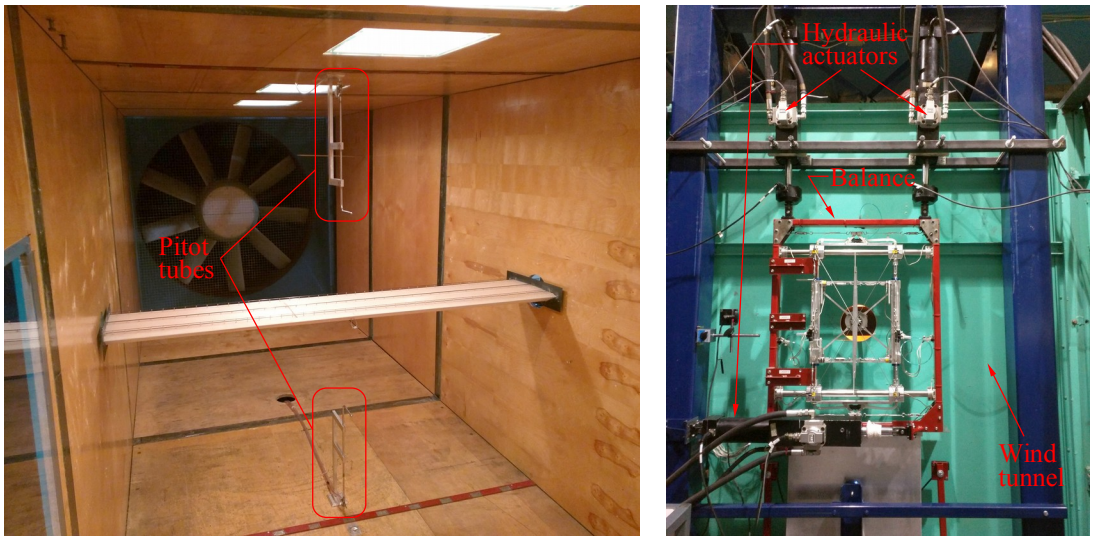

(a) Model mounted on the aerodynamic balance (inside the wind tunnel)

(b) Aerodynamic balance set for forced-vibration tests (outside the wind tunnel)

FIGURE 2 - Experimental setup

Section Models

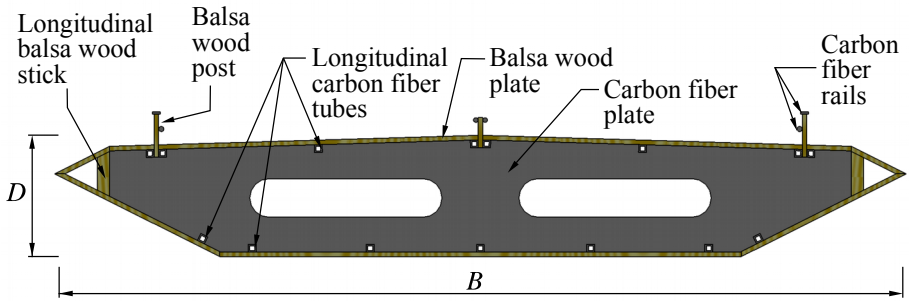

FIGURE 3 - Typical model cross section

For this investigation on extraction parameters of flutter derivatives, three section models of the Great Belt Bridge were built for three different scales. The geometry of the models comes from [9]. For the models, a frame made of carbon fiber was built. This frame was covered by balsa wood plates as illustrated in Fig. 3. The properties of the models are presented in Tab. 1. The models are light as demon-

strated by their mass (m_{model}) in Tab. 1. A low mass was required in order to decrease the inertial forces of the models measured by the aerodynamic balance. This ensures a more precise identification of flutter derivatives when the forced-vibration procedure is used. To minimize the vibration of the models during the forced-vibration tests, the frequency f_{model} of the fundamental mode (vertical) is much higher than the maximum frequency of oscillation imposed to the models (GB1 7.8 Hz, GB2 5.3 Hz, GB3 3.9 Hz). The frequency f_{model} was obtained using a finite element model of the section model mounted on the test rig. Beam elements were used for this purpose. More details on the section models are provided in [8].

TABLE 1 - Properties of the Great Belt Bridge models

Model	Scale	Width B (mm)	Depth D (mm)	Length L (mm)	Mass m_{model} (kg)	Freq. f_{model} (Hz)
GB1	1:140	226	31	1808	1.47	25.1
GB2	1:95	330	46	1805	1.90	37.1
GB3	1:70	448	63	1806	1.72	41.7

Harmonic Forced-Vibration Tests

The first step of this study on the extraction parameters was to identify the flutter derivatives using harmonic forced-vibration tests. For these tests, uncoupled sinusoidal motions were imposed to the model, i.e., along one DOF (p , h or α). Tests were performed for multiple wind speeds to obtain curves for the flutter derivatives. Some tests were also conducted without wind in order to isolate the aerodynamic component of the measured forces, which include the inertial forces. The identification procedure used for the flutter derivatives is based on a linear least-squares approach, and is described in [8]. From the measured aerodynamic forces, the flutter derivatives are obtained considering the experimental amplitude and frequency of oscillation in the identification procedure.

TABLE 2 - Test parameters for the harmonic tests (model scale)

DOF x	RMS velocity $\dot{x}_{rms}$				Amplitude x_o			
	1	2	3		A	B	C	
p	46	67	88	mm/s	$B/74$	$B/52$	$B/40$	-
h	46	67	88	mm/s	$B/74$	$B/52$	$B/40$	-
α	15	22	29	°/s	1.0	1.5	2.0	°

As mentioned earlier, the studied parameters are the model scale, model velocity and amplitude of motion. The velocities and amplitudes used for the harmonic tests are shown in Tab. 2. For harmonic tests, the velocity is also harmonic. Thus, an effective velocity, the RMS velocity (root mean square), was used in this parametric study. The relationship between the frequency of oscillation used in harmonic tests and the RMS velocity is given by Eq. 4. For each RMS velocity, three amplitudes were tested for a total of nine test configurations for each DOF. The tests for these configurations were performed for the models GB1, GB2 and GB3 to assess the effect of scale on the flutter derivatives.

$$f_x = \frac{\dot{x}_{rms}\sqrt{2}}{2\pi x_o} \tag{4}$$

where f_x is the frequency of oscillation ($x = p, h, \alpha$); $\dot{x}_{rms}$ is the RMS velocity; x_o is the amplitude of motion.

Forced-Vibration Tests at Absolute Constant Velocity

To have a better understanding of the effect of velocity on the flutter derivatives, forced-vibration tests at absolute constant velocity similar to [7] were also performed. For such tests, an uncoupled triangular wave motion as illustrated in Fig. 4 is imposed to the model. As shown in Fig. 4, parabolic transitions were used to facilitate the change of direction of the model. For the measurements of flutter derivatives, a similar procedure as for the harmonic tests was used. It should also be noted that the parabolic transitions were not considered in the identification procedure.

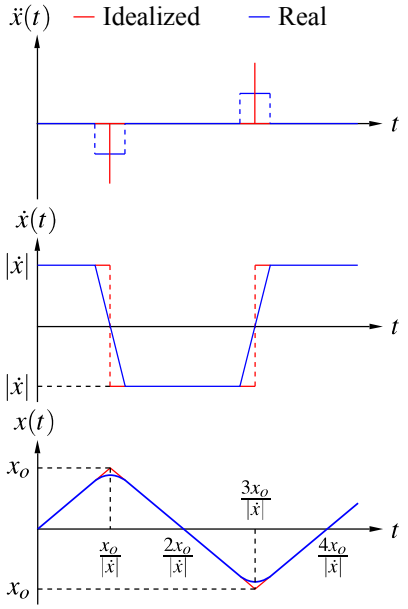

FIGURE 4 - Absolute-constant-velocity motion

The test parameters used for the absolute-constant-velocity tests are given in Tab. 3. Five absolute velocities were tested, and for each absolute velocity, two amplitudes were employed for a total of ten test configurations for each DOF. The models GB1, GB2 and GB3 were used for these tests.

TABLE 3 - Test parameters for the absolute-constant-velocity tests (model scale)

DOF x	Absolute velocity $\lvert\dot{x}\rvert$						Amplitude x_o		
	1	2	3	4	5		A	B	
p	40	65	90	115	140	mm/s	$B/49$	$B/33$	-
h	40	65	90	115	140	mm/s	$B/49$	$B/33$	-
α	8	16	24	32	40	°/s	2.0	3.0	°

RESULTS

Flutter Derivatives from Harmonic Tests

Before the assessment of the extraction parameters on flutter derivatives, it is relevant to mention that the flutter derivatives measured at the *Université de Sherbrooke* for the Great Belt Bridge were found to be in good agreement with the published ones [9]. For the study on extraction parameters, the polynomial curve fits of the flutter derivatives were used in order to facilitate the analysis. Additionally,

due to the difficulty to measure precisely most of the derivatives P_i^*, they are not presented in the following figures.

First, the effect of model scale is analyzed by comparing the flutter derivatives measured for the models GB1, GB2 and GB3. Fig. 5 presents selected flutter derivatives of these models for the test configuration S2B, which refers to a harmonic test configuration with RMS velocity 2 and amplitude B. In this figure, similar trends for H_5^*, H_1^*, A_2^* and A_3^* are observed when curves for different scales are compared. Similar observations were also made for other flutter derivatives (H_i^* and A_i^*) and other test configurations of Tab. 2 [8]. Therefore, the nondimensionalization of Scanlan's formulation with respect to the bridge-deck width is satisfactory in general. Nevertheless, discrepancies can be noticed in Fig. 5 for H_6^* and A_4^*, which are flutter derivatives relative to the displacements. It is impossible to say these discrepancies are caused by the model scale because these derivatives include the aerodynamic mass. This is due to the fact that the displacements and accelerations are linearly dependent for harmonic tests. In addition, for a same RMS velocity and amplitude of motion, models with different scales are submitted to different accelerations. Therefore, the scale or acceleration could be responsible for the discrepancies. Similar discrepancies were also observed for other flutter derivatives relative to the displacements, e.g., H_4^* and A_6^*.

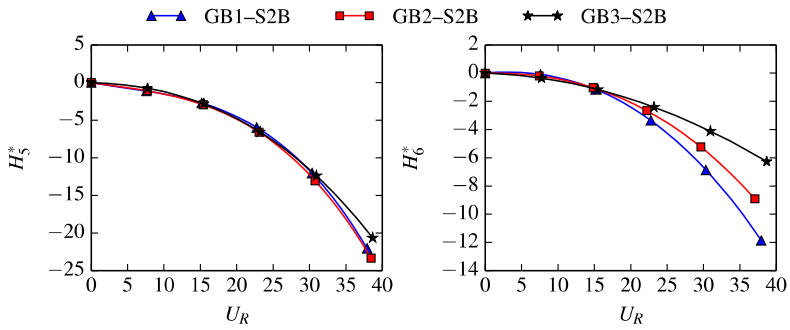

(a) Horizontal motion

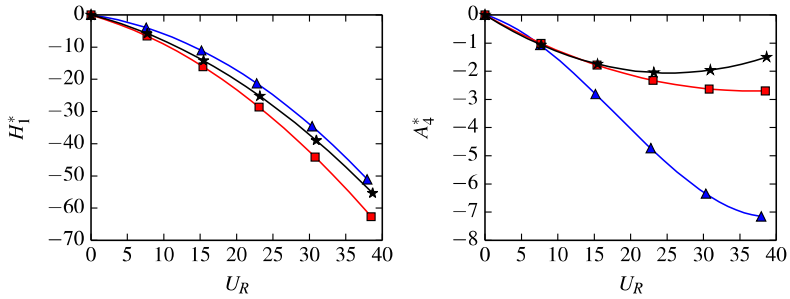

(b) Vertical motion

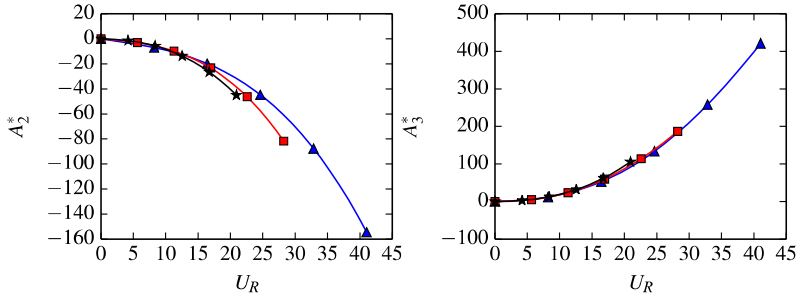

(c) Rotational motion

FIGURE 5 - Effect of scale on the flutter derivatives

Then, the effect of RMS velocity and amplitude of motion is assessed in Fig. 6. For this purpose, selected flutter derivatives for the nine harmonic test configurations (Tab. 2) are compared in the case of the model GB3. In Fig. 6, we denote the different curves of H_1^*, A_4^* and A_3^* are very similar, which was also observed for other flutter derivatives (P_5^*, P_6^*, H_3^*, H_4^* and A_1^*). A dependence for the amplitude is seen for H_6^* (also observed for A_6^*). This could be attributed to the effect of amplitude on the acceleration of the deck since the aerodynamic mass is included in H_6^* and A_6^*. Additionally, H_5^* and A_2^* show nonlinearities with respect to the RMS velocity or amplitude (also observed for H_2^* and A_5^*). Nevertheless, it is not possible to say which of these parameters caused the nonlinearities for these derivatives because the flutter derivatives are nondimensionalized with respect to the frequency of oscillation. Similar conclusions regarding the RMS velocity and amplitude were obtained for the models GB1 and GB2.

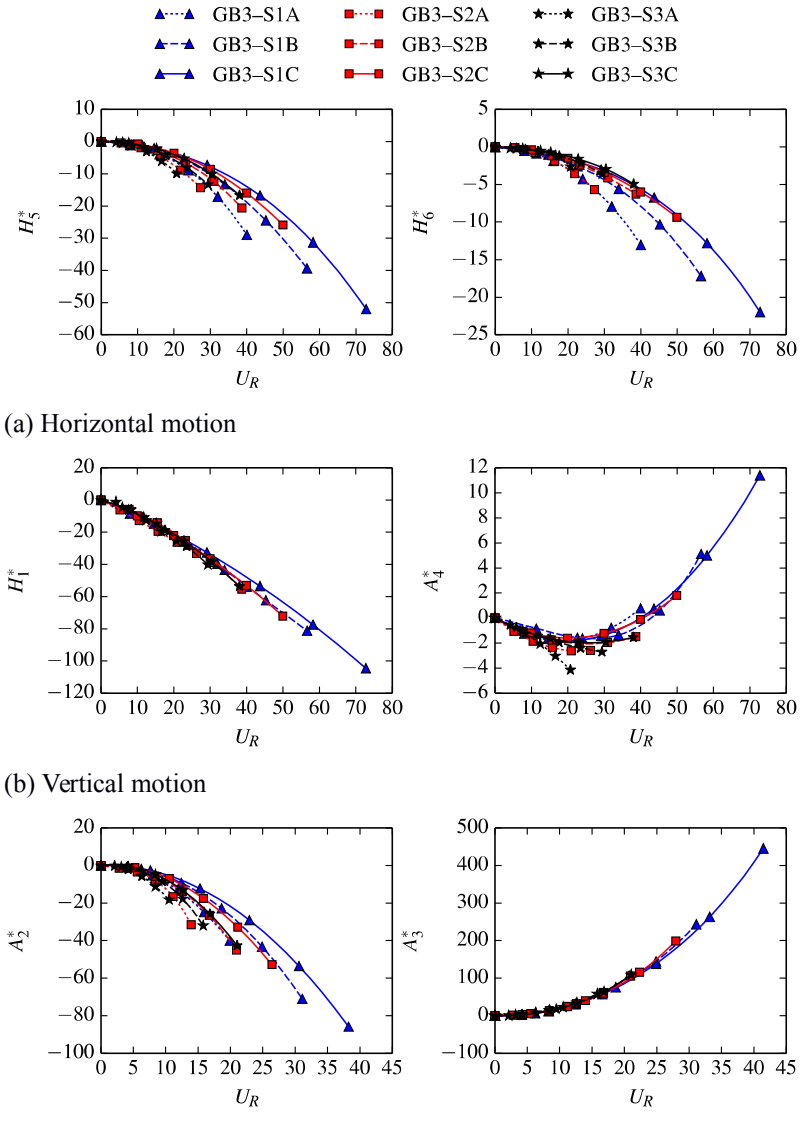

(a) Horizontal motion

(b) Vertical motion

(c) Rotational motion

FIGURE 6 - Effect of RMS velocity and amplitude on the flutter derivatives

To have a better understanding of the nonlinearities of H_5^* and A_2^* with respect to the RMS velocity and amplitude, these flutter derivatives for the model GB3 are studied in their dimensional form. In Fig. 7a, the curves for the RMS velocity 1, 2 and 3 are shown for the amplitude B. The curves for the amplitude A, B and C are presented for the RMS velocity 2 in Fig. 7b. In Fig. 7a, the nonlinear behav-

ior of H_5 and A_2 with respect to the RMS velocity can be seen. According to Fig. 7b, only A_2 shows a slight dependence for the amplitude. Therefore, the nonlinearities observed for H_5^* and A_2^* are mainly caused by the RMS velocity. Similar conclusions were obtained for H_2^* and A_5^*.

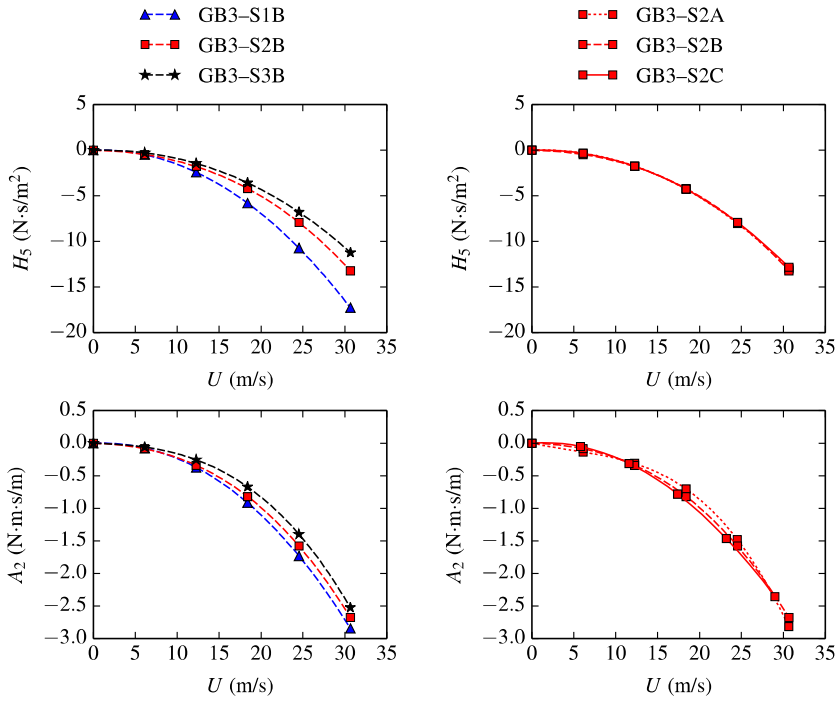

(a) Effect of RMS velocity (b) Effect of amplitude

FIGURE 7 - Dimensional flutter derivatives obtained from harmonic tests

Flutter Derivatives from Absolute-Constant-Velocity Tests

As mentioned previously, absolute-constant-velocity tests were performed in order to have a better assessment of the effect of velocity on the flutter derivatives. First, it is relevant to mention the flutter derivatives measured using absolute-constant-velocity tests compare well to the ones obtained from harmonic tests when studied in dimensional form [8]. For the flutter derivatives obtained from the absolute-constant-velocity tests, similar curves are obtained for the different amplitudes of Tab. 3. Consequently, the following analysis focuses on the effect of velocity on the flutter derivatives. From the observations made for the RMS velocity in Fig. 7a, the effect of the velocity is studied in Fig. 8 for H_5, A_5, H_2 and A_2 (dimensional form). In this figure, the flutter derivatives of the model GB3 measured using the absolute-constant-velocity tests are presented for the five velocities and amplitude B. This figure shows a clear dependence of these flutter derivatives with respect to the velocity, which confirms the observations made in Fig. 7a. These conclusions indicate the importance of the model velocity on the flutter derivatives. Thus, it would be interesting to study a new nondimensionalization for the flutter derivatives based on the velocity.

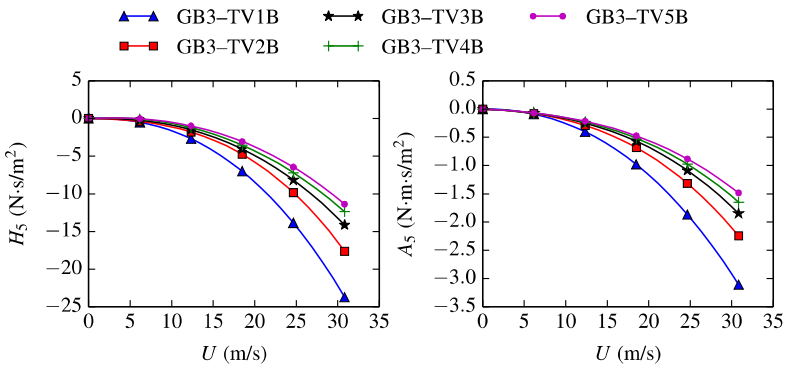

(a) Horizontal motion

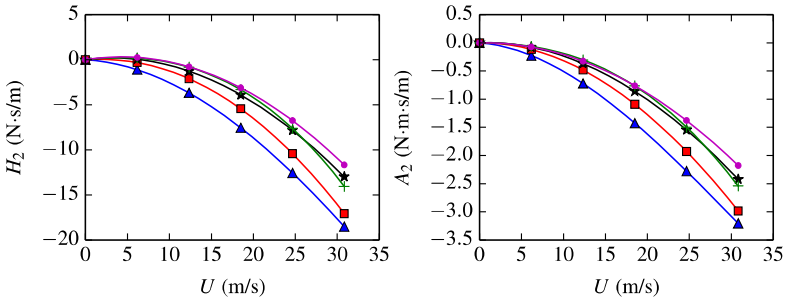

(b) Rotational motion

FIGURE 8 - Effect of velocity on the dimensional flutter derivatives obtained from absolute-constant-velocity tests

CONCLUSIONS

Scanlan's formulation of self-excited forces is commonly used for the flutter analysis of bridges, but its use is limited to linear analyses. The first step in the development of a new time-domain model, which will allow nonlinear analyses, was to perform a parametric study on the extraction parameters used in wind tunnel for the identification of flutter derivatives. The effect of the model scale, model velocity and amplitude of motion was assessed by carrying out forced-vibration tests for three section models with different scales. Harmonic and absolute-constant-velocity tests were conducted for many test configurations.

The flutter derivatives measured for different model scales show similar trends, which confirms the nondimensionalization of flutter derivatives with respect to the bridge-deck width. A dependence for the amplitude of motion was observed for selected flutter derivatives (e.g. H_6^* and A_6^*). Also, the flutter derivatives H_5^*, A_5^*, H_2^* and A_2^* show nonlinearities for the velocity when the dimensional form is used. Therefore, a new nondimensionalization for the flutter derivatives based on the velocity could lead to the development of a new time-domain formulation of self-excited forces similar to Scanlan's formulation. Such a time-domain model could be used to perform nonlinear flutter analysis and investigate the effect of different nonlinearities on the flutter wind speed.

ACKNOWLEDGEMENT

The financial support of the Natural Sciences and Engineering Research Council of Canada (NSERC) and the *Fonds de recherche du Québec - Nature et technologies* (FRQNT) was greatly appreciated for the realization of this research project.

REFERENCES

[1] R.H. Scanlan, J.J. Tomko, 1971, "Airfoil and bridge deck flutter derivatives", *J. Eng. Mech. Div*. vol. 97, 1717-1737.

[2] M. Falco, A. Curami, A. Zasso, 1992, "Nonlinear effects in sectional model aeroelastic parameters identification", *J. Wind Eng. Ind. Aero.* vol. 42, 1321-1332.

[3] G.L. Larose, A.G. Davenport, J.P.C. King, 1993, "On the unsteady aerodynamic forces on a bridge deck in turbulent boundary layer flow", *Proceedings 7th U.S. National Conference on Wind Engineering*, 373-382.

[4] Z. Chen, X. Yu, G. Yang, B. Spencer, 2005, "Wind-induced self-excited loads on bridges", *J. Struct. Eng*. vol. 131, 1783-1793.

[5] P.P. Sarkar, N.P. Jones, R.H. Scanlan, 1994, "Identification of aeroelastic parameters of flexible bridges", *J. Eng. Mech.* vol. 120, 1718-1742.

[6] S. Prud'homme, F. Legeron, A. Laneville, 2015, "Effect of sway movement and motion axis on flutter and vortex induced vibration in a 3 DOF wind tunnel sectional test", *J. Wind Eng. Ind. Aero.* vol. 136, 82-88.

[7] S. Prud'homme, F. Legeron, A. Laneville, 2015, "Transient flutter analysis of bluff bodies", *J. Wind Eng. Ind. Aero.* vol. 145, 139-151.

[8] S. Maheux, 2017, *Simulation dynamique du flottement d'un pont élancé à l'aide de coefficients instationnaires temporels,* Master's thesis, Université de Sherbrooke, Sherbrooke, Canada, 190.

[9] T.A. Reinhold, M. Brinch, A. Damsgaard, 1992, "Wind tunnel tests for the Great Belt Link", *Proceedings Aerodynamics of Large Bridges*, 255-267.